Assimilation of chlorophyll data into a stochastic ensemble simulation for the North Atlantic Ocean

Yeray Santana-Falcón[1,2], Pierre Brasseur[1], Jean Michel Brankart[1], and Florent Garnier[3]

[1]Université Grenoble Alpes, CNRS, IRD, Grenoble INP, IGE, (Grenoble), France
[2]CNRM, Université de Toulouse, Météo-France, CNRS, Toulouse, France
[3]LEGOS, University of Toulouse, CNRS, IRD, CNES, UPS, (Toulouse), France

Correspondence: Yeray Santana-Falcón (yeray.santana-falcon@univ-grenoble-alpes.fr)

Abstract.

Satellite-derived surface chlorophyll data are assimilated daily into a three-dimensional 24 member ensemble configuration of an online-coupled NEMO-PISCES model for the North Atlantic Ocean. A one-year multivariate assimilation experiment is performed to evaluate the impacts on analyses and forecast ensembles. Our results demonstrate that the integration of data improves surface analysis and forecast chlorophyll representation in a major part of the model domain, where the assimilated simulation outperforms the probabilistic skills of a non-assimilated analogous simulation. However, improvements are dependent on the reliability of the prior free ensemble. A regional diagnosis shows that surface chlorophyll is overestimated in the northern limit of the subtropical North Atlantic, where the prior ensemble spread does not cover the observation's variability. There, the system cannot deal with corrections that alter the equilibrium between the observed and unobserved state variables producing instabilities that propagate into the forecast. To alleviate these inconsistencies, a one-month sensitivity experiment in which the assimilation process is only applied to model fluctuations is performed. Results suggest the use of this methodology may decrease the effect of corrections on the correlations between state vectors. Overall, the experiments presented here evidence the need of refining the description of model's uncertainties according to the biogeochemical characteristics of each oceanic region.

1 Introduction

Estimating the biogeochemical state of the ocean has become fundamental under the current climate change context due to its key role mediating global carbon stocks (e.g., Houghton et al., 2001). Currently, the optimal combination of observational data with the dynamical equations embedded in models through data assimilation (DA) is the most comprehensive strategy to meet this goal. Therefore, there is a growing effort towards the development of effective DA techniques to improve hindcasts, forecasts, nowcasts, and scenario simulations of ocean biogeochemistry (e.g., Brasseur et al., 2009; Yu et al., 2018; Fennel et al., 2019). At present, the Copernicus Marine Environment Monitoring Service (CMEMS) delivers DA biogeochemical products for only selected regions (von Schuckmann et al., 2019), though the operational production of the data-assimilated biogeochemical state of the ocean is one of its challenging core objectives.

In order to achieve model / data integration it is of utmost importance to explicitly identify the structure of the uncertainties that affect the model and the observations (Lahoz et al., 2010). In this sense, ensemble methods (e.g., Bessières et al., 2017) are designed to provide a statistical description of the inaccuracies associated with a complex model system by describing the evolution of the probability density function (PDF). An appropriate approach to perform ensemble simulations is by introducing stochastic noise into the (deterministic) model equations to simulate the effect of the uncertainties. Stochastic parameterizations have been used in meteorological forecasting (e.g., Buizza et al., 1999; Leutbecher et al., 2017), and are becoming the standard procedure for climate modelling (see Palmer, 2012; Berner et al., 2017). In oceanography, the implementation of this type of probabilistic approach has increased in the last decade (e.g., Brankart et al., 2015; Juricke et al., 2017), although its application in physical-biogeochemical models is quite unusual.

In a precursory study, stochastic perturbations were applied into a deterministic solution of the Mercator Ocean (http://www.mercator-ocean.fr.) North Atlantic 1/4° configuration of the NEMO-PISCES coupled model to parameterize selected model uncertainties associated with some poorly-resolved processes (see Garnier et al., 2016, for more details). Ensemble simulations involving 60 members were performed using a probabilistic version of the NEMO-PISCES simulation for the year 2005. An objective diagnosis of this ensemble simulation showed its probability distribution is quite consistent with ocean color observations in the most productive regions of the North Atlantic, a prerequisite to undertake DA applications.

Ocean color data have been successfully used in DA procedures for improving the simulation of nutrients and primary production in ocean models (e.g., Gregg, 2008; Ciavatta et al., 2011; Ford et al., 2012; Fontana et al., 2013; Teruzzi et al., 2018). However, none of the latter studies explicitly incorporates the uncertainties in the ocean biogeochemistry introduced by stochastic approaches on the model formulation. In this context, the overarching aim of the present work is to investigate to what extent the parameterizations developed in Garnier et al. (2016) can be implemented to build a complete 4D assimilation system using ocean color data that will update the state-of-the-art of biogeochemical DA. Our strategy will rely on the daily integration of surface chlorophyll (Chl-*a* hereafter) data within the latter probabilistic solution. To that end, 24 trajectories of the original ensemble are daily updated by a square root algorithm based on the SEEK (singular evolutive extended Kalman) filter (Pham et al., 1998; Brasseur and Verron, 2006) using daily composites of ocean colour observations extracted from MERIS (MEdium Resolution Imaging Spectrometer). Following this strategy, a one year experiment is performed in order to investigate the effects of the assimilation in contrasted periods (e.g., bloom vs nutrient-depleted periods) throughout the annual cycle.

The paper is structured as follows: section 2 presents the coupled model, the assimilation scheme, and the validation metrics. Section 3 presents the results of the experiment, and provides a probabilistic assessment as compared it with a non-assimilated ensemble simulation. A discussion of the most relevant outputs is carried out in section 4. In particular, we assess how the DA system based on parameterized uncertainties can reduce the model uncertainties, and evaluate its performance at selected regions. Lastly, a summary, conclusions and future perspectives are proposed in section 5 in which we suggest directions for next possible developments.

2 Material and methods

2.1 Hydrodynamical model

The assimilation system presented here is based on a realistic three-dimensional physical-biogeochemical simulation. The physical component is simulated using the primitive equation free-surface ocean circulation model NEMO (Nucleus for European Modeling of the Ocean, version 3.4; Barnier et al., 2006; Madec et al., 2015), whose prognostic variables are temperature, salinity and the three-dimensional velocity fields.
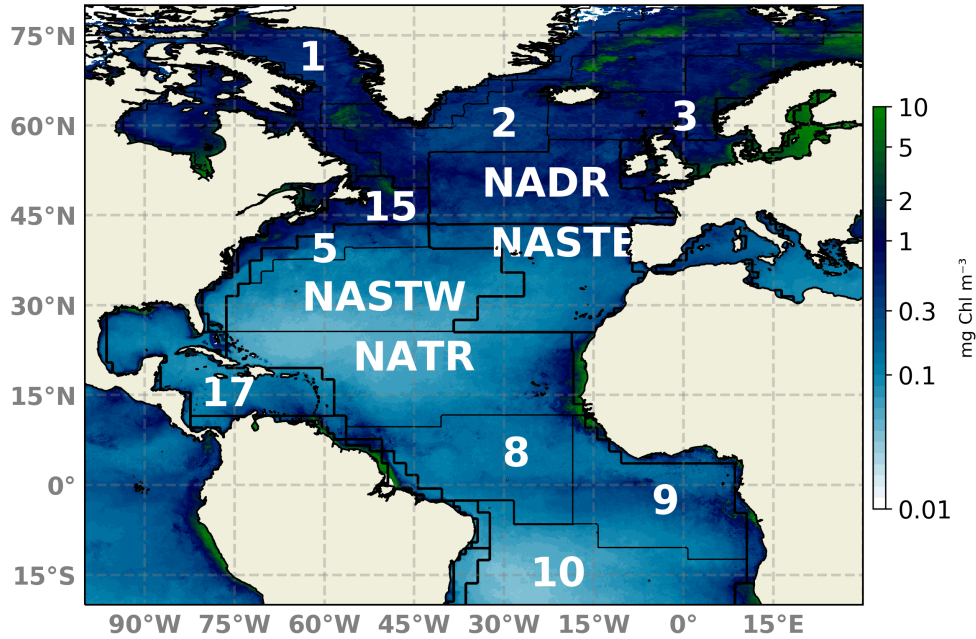

Figure 1. Schematic map of the North Atlantic basin showing the *NATL-025/PISCES* domain. Longhurst et al. (1995) biogeochemical provinces are indicated and numbered. Provinces indicated by acronyms NADR (North Atlantic Drift), NATR (North Atlantic tropical gyre), NASTE (Northeast Atlantic subtropical gyre), and NASTW (Northwest Atlantic subtropical gyre) are used throughout the text. A 2018 yearly composite of sea surface Chl-*a* is superimposed.

The model configuration is a duplicate of the North Atlantic configuration developed within the framework of the project DRAKKAR (referred to here as NATL025; Barnier et al., 2006, https://www.drakkar-ocean.eu), which covers the North Atlantic region from 20° S to 80° N and 98° W to 23° E (*Fig.* 1). The numerical grid has a horizontal resolution of a quarter of degree, and 46 geopotential levels in the vertical from surface to 6000 m depth. Such an eddy-permitting resolution enables some rough representation of mesoscales features, which are key elements for primary production (Oschlies and Garçon, 1998; Lévy et al., 2012). The dynamical component is forced by ERA-INTERIM atmospheric fields (Simmons, 2006; Dee

et al., 2011). This configuration has already been coupled to biogeochemistry modules and evaluated in recent numerical
70 studies (e.g., Ourmières et al., 2009; Doron et al., 2011, 2013; Fontana et al., 2013; Garnier et al., 2016).

2.2 Biogeochemical model

The biogeochemical component coupled to hydrodynamics is PISCES (Pelagic Interaction Scheme of Carbon and Ecosystem
Studies, version 2; Aumont et al., 2015). PISCES is a complex carbon-based model that simulates marine biological produc-
tivity and carbon biomass based upon five main nutrients: nitrate, ammonium, phosphate, silicate and iron. Its architecture
75 includes 24 biogeochemical variables grouped into four main compartments: nutrients, phytoplankton, zooplankton, and detri-
tus. PISCES has been used in global simulations (e.g., Bopp et al., 2015), environmental studies (e.g., Brasseur et al., 2009),
climate studies (Lefort et al., 2015), basin scale studies (e.g., Jose et al., 2014) and, more recently, in regional scale studies
(e.g., Auger et al., 2015). For more details see Aumont et al. (2015) where a complete description of PISCES equations along
with a brief validation are presented.

80   PISCES differentiates two phytoplankton functional types: diatoms and nanophytoplankton. The parameterization of di-
atoms differs from nanophytoplankton in their requirements of silicate (Si), an increased consumption of iron (Fe), and a
higher level of nutrient saturation due to its larger size. Both Chl-*a* content on nanophytoplankton and diatoms are param-
eterized using the photo-adaptative model of Geider et al. (1997). We refer Chl-*a* to here as the direct sum of these two
compartments, and it will be used as a proxy for primary production. Besides biomass of Chl-*a*, carbon ratios with Fe, and Si
85 (only for diatoms) are explicit prognostic variables of the model. Furthermore, PISCES discretises two sizes of zooplankton:
micro- and mesozooplankton, and three classes of non-living compartments: the semi-labile dissolved organic carbon pool,
and two sizes of particulate organic carbon that differ by their sinking velocities (3 m d^{-1} for small particles, and 50 to 200 m
d^{-1} for large particles).

A realistic dynamical adjustment of the modeled ocean state is obtained after a 13 years spin-up (1989-2002) starting from
      PISCES is coupled on-line to NEMO with a coupling frequency equal to the circulation model time-step (i.e., 40 min). Note
90 that on-line coupling means here one-way forcing of the ecosystem model by the circulation model, since no feed-back of the
ecosystem model is taken into account. This strategy of on-line coupling with a maximum frequency is thought to be useful
for simulating the ecosystem evolution, while avoiding possible problems brought by the use of averaged physical fields, as in
off-line coupling.

      A realistic dynamical adjustment of the modeled ocean state is obtained after a 13 years spin-up (1989-2002) starting from
95 the Levitus climatology for temperature and salinity (Levitus et al., 1998). After physical spin-up, the biogeochemical compo-
nent is initialized in January 2002 from outputs of a global 1/4° PISCES operational simulation performed by MERCATOR
Ocean (Elmoussaoui et al., 2011). Between January 2002 and December 2004, a three years spin-up is performed to ensure a
consistent biological initial state. After this period, a deterministic simulation of the coupled system, i.e., NATL025-PISCES,
is performed for a period of six years, extending from January 2005 to December 2010. This simulation is used to build a
100 probabilistic configuration upon which a data assimilation system is performed.

2.3 Probabilistic version of the coupled system

Any realistic description of the state of a system involves uncertainties. In the case of coupled ocean models, uncertainties may originate from external forcings (e.g.,the atmospheric data), parameterizations of physical and biological processes that are not explicitly resolved by the model, omission of unresolved scales, and reduced complexity to limit computational costs. In a previous study (Garnier et al., 2016), two classes of those uncertainties were parameterized to explicitly simulate the errors associated with the deterministic model formulation; (1) the limitations of the spatial scales resolved by the model, and (2) the simplification of the description of the biogeochemical system to a limited number of state variables and parameters. The first ones were described by following the approach proposed in Brankart et al. (2015), and the second ones were simulated by introducing log-normal stochastic perturbations on seven key biogeochemical parameters whose uncertainties may have a direct impact on the estimation of primary production. Specifically, the parameters perturbed are the phytoplankton growth rate at 0º C, the initial P-I slope for both nanophytoplankton and diatoms, the phytoplankton temperature sensitive of growth, the zooplankton temperature sensitive of grazing and the growth dependency to the day length for both nanophytoplankton and diatoms. For the perturbations, the starting point is a first-order autoregressive process setting up with a standard deviation of 0.3 and a decorrelation time scale of 1 month, at which a random noise is drawn at each grid point and at each time step. After spatial filtering, Gaussian noises are transformed in Lognormal noises to guarantee positivity. Stochastic perturbations are then introduced by multiplying by these Lognormal noises. To preserve vertical consistency, all perturbations are set identical for the whole water column. In addition, as the effects of unresolved scales will have an impact on the large scale biogeochemical representation, we create a perturbation that simulates the unresolved fluctuation of the concentration of each parameter within every model grid box.

The stochastic formulation was introduced to produce an ensemble spread that is large enough for building a DA system while keeping the coupled model stable. A 60 member ensemble simulation for year 2005 was performed by Garnier et al. (2016) who show that the resulting probability distribution (of the annual ensemble simulation) is quite consistent with SeaWiFS (Sea-viewing Wide Field-of-View Sensor) ocean color observations. Specifically, they assessed the reliability or statistical consistency of the ensemble simulation by comparing it with satellite Chl-*a* data assuming 30% of observation error.

The present study is based on these previous developments, with some additional adjustments to prepare for DA. In particular, we carried out sensitivity experiments to select an ensemble size that is more cost-efficient, but with the same level of agreement to observations as in Garnier et al. (2016). More explicitly, 1-month assimilation experiments were performed by reducing the ensemble size from the original 60 members to 12 and 24 members. We first compared each of them with the original experiment, and observed surface Chl-*a* differences below 0.5 mg Chl m^{-3} for most regions between the 24 and the 60 member ensembles. A comparison against the observations used for the assimilation process was also assessed. Both reduced ensemble simulations were able to reproduce the main patterns of surface Chl-*a* displayed by satellite observations. However, global probabilistic metrics showed that only the 24 member ensemble experiment conserves the same level of statistical consistency as the original ensemble, while reducing computational costs of the forecast step by up to 60%. The probability distribution of the 12 member ensemble showed an underdispersed distribution, while the 24 member ensemble showed the ensemble spread

135 covers a major part of the observations. Therefore, a total of 24 trajectories of the inherited stochastic simulation developed by Garnier et al. (2016) are used here as the prior PDF for the assimilation problem.

2.4 Assimilation scheme

The assimilation system integrates daily composites of MERIS Chl-*a* observations to daily update the ensemble forecast. The methodology behind this process is based onto a SEEK filter (Pham et al., 1998; Brasseur and Verron, 2006), implemented in
140 the ensemble system using the System of Sequential Assimilation Modules (SESAM) assimilation platform (Brankart et al., 2012) that deals with all matrix operations required by the assimilation scheme. Though using a probabilistic approach is more resource-costing, it produces a probability distribution that allows for an objective validation with observations using probabilistic scores, unlike a deterministic assimilation system that provides only one estimated trajectory. As another advantage, the explicit simulation of model uncertainties in the ensemble approach is necessary to produce a description of uncertainties
145 that is consistent with observations.

The assimilation scheme proceeds in two steps. (1) An ensemble forecast in which each ensemble member, i.e., state vector, is propagated forward in time using the full model equations. (2) When a set of observations, i.e., daily swaths of ocean color retrieved from MERIS, is available, the statistical information contained in the ensemble is combined with observations to update the forecasted ensemble. The most relevant aspects of this second step, referred to as analysis, will be commented on
150 below. To propagate the system, the initial condition of the subsequent daily forecast is the updated analysis ensemble obtained by the assimilation of Chl-*a* observations.

The state vector entering the analysis step is composed of all prognostic biogeochemical state variables of the three-dimensional grid following a multivariate approach. To keep the analysis computationally affordable, a prior diagnosis of the multivariate correlations between the observed (Chl-*a* in this case) and non-observed biogeochemical variables have been
155 carried out. Following the results obtained from this test, 12 out of the 24 biogeochemical state variables are included into the updated state vector. These state variables correspond to nutrients, oxygen, zooplankton, phytoplankton, and Chl-*a*.

The probability distribution of the observed variable, i.e., Chl-*a*, is usually considered as log-normal (Campbell, 1995). A well-known strategy to accommodate the characteristic non-Gaussian distributions of biogeochemical parameters is applying a log-normal transformation (e.g., Ciavatta et al., 2011; Mattern et al., 2017). However, this transformation assumes that the
160 shape of the probability distribution does not change. As this is not often verified, we adopted here another non-linear strategy dependent on the shape of the probability distribution. Anamorphosis transformations (Bertino et al., 2003; Béal et al., 2010) are applied to each variable of the state vector prior to the ensemble analysis step to ensure that marginal PDFs are close to Gaussian. The strategy of these transformations relies on remapping the quantiles of each marginal distribution such that the probability distribution is as close as possible to a Gaussian. These transformations ensure that no value of the vari-
165 ables becomes negative after the analysis update, improve the description of the correlations between Chl-*a* and non-observed variables, and exclude possible causes of breakdown of the simulation. To be compliant with the new variables, observations are also transformed into the anamorphic space defined by the ensemble simulation. After analysis, the corresponding inverse transformations are performed to come back into the original model space and initialize the subsequent daily ensemble forecast.

Relatively small ensembles like the one used here can lead to spurious correlations between distant model grid points. In order to avoid the potential negative effects of these correlations, we employ a domain localization methodology in which a separate analysis for each local domain is applied. In practice, this means that an analysis update is performed for each horizontal grid point, but including all vertical levels and state variables. To ensure continuity between analyses, each analysis uses the observations within a certain localization radius (of one degree in the present case), with an observation error that increases with distance.

2.5 Assimilated and independent observations

The observation data set assimilated by our system corresponds to daily swaths of ocean color retrieved from MERIS. Specifically, we use Level-3 binned data accessible at http://earth.esa.int/level3/meris-level3/, that consist on daily-accumulated Level-2 products with standard bin size of 4.6 km. Among other properties, this product provides Chl-*a* estimations (in mg Chl m^{-3}) used here to update the ensemble simulation. Additionally, the system performance will be assessed by comparison with ocean color SeaWiFS data accessible through https://oceancolor.gsfc.nasa.gov/data/seawifs/, and with daily surface Chl-*a* fields obtained from the Global Ocean Satellite Observations provided by Copernicus-GlobColour service, and accessible through http://marine.copernicus.eu. This latter product is based on the merging of several sensors (Data from SeaWiFS, MODIS-Aqua, and MERIS sensors are used for year 2005) delivered at 4 km of spatial resolution.

The limited accuracy of ocean color products is taken into account in the assimilation process. Imperfections in the retrieval process of the Chl-*a* concentrations may be due to the presence of chromophoric dissolved organic matter, atmospheric aerosols, or errors in the algorithms at some specific regions, among others (e.g., Gregg and Casey, 2004; Le Fouest et al., 2006). Therefore, a 30% of observational error is considered in agreement with global average standard deviation estimates (e.g., Gregg and Casey, 2004; Mélin et al., 2016).

While inter-comparisons between the data-assimilated simulation and the assimilated observations are necessary to assess the experiment efficiency, the validation strategy is not totally conclusive since they are not independent (Gregg et al., 2009). We thus use an additional independent data set for an objective validation of the assimilation process. Specifically, we use biogeochemical fields extracted from the World Ocean Atlas 2018 (WOA2018; Garcia et al., 2019). The historical *in situ* nutrient measurements available in this data set were produced by the NOAA's (National Oceanic and Atmospheric Administration) National Oceanographic Data Center - Ocean Climate Laboratory as part of the World Ocean Database project (WOD; Boyer et al., 2013). They will be used to assess the simulation performance on matching the non-observed variables patterns.

2.6 Probabilistic validation

Unlike for deterministic simulations, the validation of our DA experiment requires many realizations (members) to be properly evaluated given its probabilistic nature. For that purpose, reliability and resolution scores (see Toth et al., 2003; Candille et al., 2015, for more information) will be computed from the ensemble. Reliability evaluates the capacity of a model to produce an ensemble probability distribution in agreement with the statistical distribution of a given observation data set. Resolution measures the ability of a model to discriminate distinct observed situations. In other words, the reliability informs of the

system's ability to produce PDFs that agree with a given observations' PDF, while resolution informs of the spread of the system's PDFs. These metrics will allow us to measure the skills of our ensemble simulation for predicting the true state of the ocean biogeochemistry.

205 To evaluate reliability and resolution, several probabilistic metrics will be employed. We first check the reliability of the DA system by introducing the rank histogram (Anderson, 1996). Rank histograms are computed by sorting all 24 members in ascending order (in the present case according to their Chl-a concentration) for each grid point and at a given date. Each observation is then ranked relatively to its location within this sorted ensemble. Observations smaller than the minimum of the ensemble will take rank '0', while those observations higher than the maximum of the ensemble will take rank 'n'. The

210 statistical consistency of the ensemble can then be evaluated by studying its shape (Candille et al., 2015; Germineaud et al., 2019). Rank histograms may be: (1) flat, which indicates the distribution of the model is accurate with the observations, i.e., perfect reliability, (2) under-dispersed or U-shaped, which indicates the spread of the ensemble is too small (too many observations lay outside the extremes of the ensemble), or (3) over-dispersed or dome-shaped, which indicates the spread of the ensemble is too large (too many observations lay near the center of the ensemble).

215 For measuring the resolution of the system, and obtain a full probabilistic validation of the ensemble, we use the continuous rank probability score (CRPS). Let x to be a parameter of interest (Chl-a in our case) to which corresponds a real observation. Then, CRPS corresponds to the distance between the simulation and the observation, as defined in

$$CRPS = E\left[\int_{\mathbb{R}} (F_p(x) - F_o(x))^2 dx\right]$$

where E is the mean over all observations at a given date, and $F_p(x)$ and $F_o(x)$, the cumulative distributions of the model and

220 the observations.

CRPS can be decomposed as the sum of the ensemble reliability (Reli) and the ensemble potential resolution (Resol), i.e., the resolution in the case of perfect reliability (see Hersbach, 2000, for more details).

$$CRPS = Reli + Resol$$

According to CRPS, a skillful probabilistic system must satisfy two criteria: Reli should be null, and Resol must tend to zero

225 and, in any case, much inferior than the reference value of the CRPS when it is only based on the reference data set (without data assimilation).

3 Results

It is instructive to evaluate how the assimilation process affects the original ensemble simulation. In this section, the impacts of the assimilation on the variability in space and time of key biogeochemical parameters are assessed by comparing the

230 assimilated experiment with an analogous 24 member ensemble of model simulations in which no observational data have been assimilated. This ensemble run is performed over the same period, and referred to as 'free run'.

3.1 Skill on reproducing surface Chl-*a*

Both the assimilated and the free run simulations are compared to daily surface Chl-*a* fields obtained from the Global Ocean Satellite Observations (see section 2.5). Merged satellite products are selected here to minimize missing data due to cloud cover
235 and still resolve mesoscale spatio-temporal variability. For the assimilated simulation, the analysis step, which corresponds to the ensemble computed after the update, is shown. Surface Chl-*a* daily composites are presented for three different dates; 19th April 2005, 15th May 2005, and 5th October 2005 (*Fig.* 2). These dates are selected for representing contrasting periods. The first two dates coincide roughly with the well documented spring-bloom period of the North Atlantic. The availability of light and nutrients during this period drives phytoplankton growth, which leads to relatively high values of Chl-*a* at surface. The last
240 date represents a period after summer when conditions change due to the reduction of sunlight over the surface.

The large-scale spatial distribution of surface Chl-*a* is captured by the DA simulation. High Chl-*a* values at regions such as the Gulf Stream, the North Sea, the Amazonian delta, and the western coast of Africa, are successfully reproduced during the first days of the experiment (*Fig.* 2 top panels). However, there is a too strong gradient between the oligotrophic conditions of the North Atlantic subtropical gyre and temperate waters to the north. The ensemble median of the free run experiment displays
245 a stronger gradient, indicating that the assimilation of surface Chl-*a* data slightly improves this situation.

About a month later (*Fig.* 2 middle panels), the inferred large-scale picture of surface Chl-*a* distribution remains close to that displayed by satellite observations. The bloom of Chl-*a* in temperate waters is well reproduced by the DA simulation both attending to magnitude and geographical location. Upwelling areas along with other zones with high Chl-*a* concentrations are also well depicted showing a good performance to match highly productive regions. By contrast, the gradient northwards of
250 the oligotrophic open ocean is too pronounced, showing no transition between both regimes as evidenced in the satellite map. Moreover, corrections made by daily satellite swaths leave imprints of their trajectory in the analysis map. These imprints are caused by using a small localization radius. This radius needs to be small due to the small correlation length scale of forecast uncertainties in the Chl-*a* field. Thus, the impact of a given observation on the update remains local. They should disappear over time as the magnitude of the innovation decreases. In this experiment, however, the time lag between observations is
255 quite large with respect (5 to 7 days) to the typical time scale of the system. By its part, the free run overestimates Chl-*a* in high-latitude regions while it underestimates it within the North Atlantic subtropical gyre.

After the summer period, at the beginning of October 2005 (*Fig.* 2 lower panels), the Chl-*a* distribution changes; regions with the highest concentrations relaxed their values, while concentrations at the open ocean slightly increased. The representation of surface Chl-*a* degrades during this period. Concentrations within the subtropical gyre agree with observations, but gradients
260 both at its northern and southern boundaries are too strong. In this transition zone, inferred values double the concentrations displayed by observations. In the rest of the domain, the Chl-*a* pattern improves that showed by the non-assimilated simulation. The free run experiment exhibits a strong overestimation at the Gulf Stream region as already observed by Garnier et al. (2016)
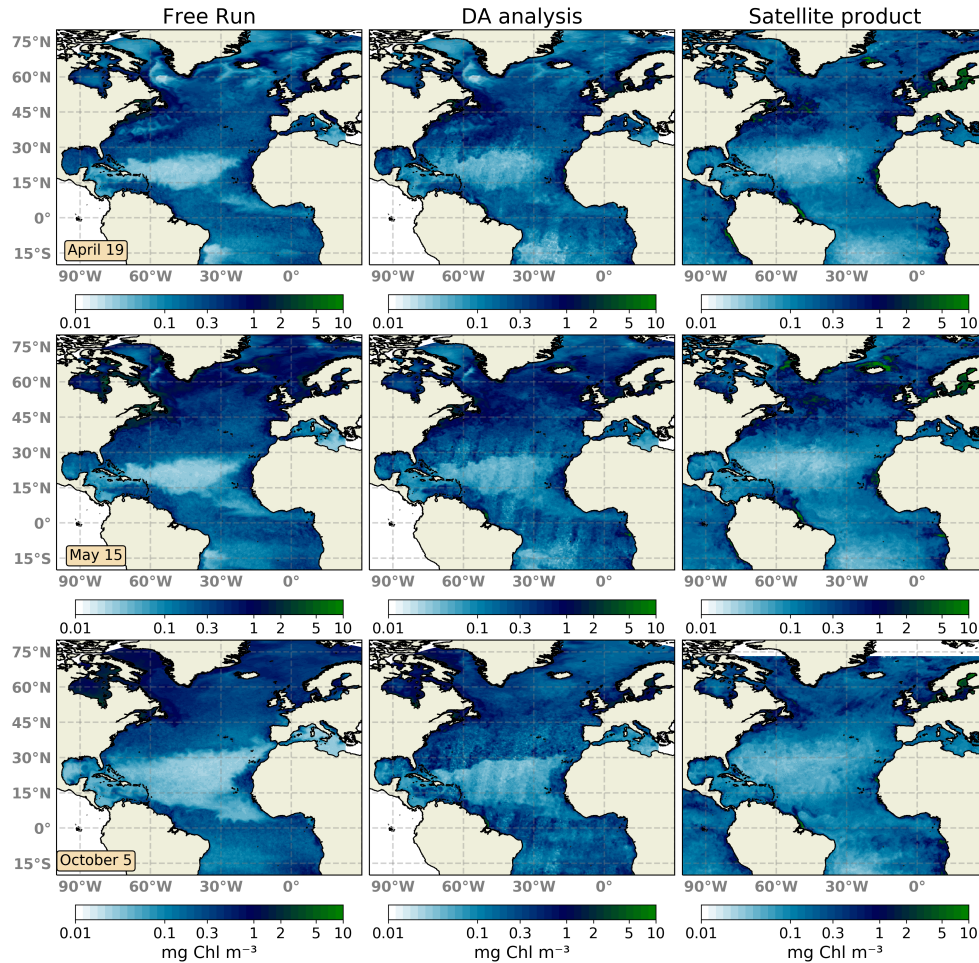
Figure 2. Surface maps of Chl-*a* (mg Chl m^{-3}) for 19th April 2005 (top panels), 15th May 2005 (middle panels), and 5th October 2005 (bottom panels). The ensemble median of the non-assimilated free run experiment (left panels), the analysis ensemble median of the assimilation experiment (middle panels), and merging daily surface Chl-*a* fields obtained from the Global Ocean Satellite Observations (right panels) are represented.

with a 60 member non-assimilated version of the coupled model. Moreover, oligotrophic conditions at the subtropical gyre are too low, which may indicate the spread of the ensemble is unable to capture the whole observation's variability.

3.2 Probabilistic regional assessment

An ensemble system should be statistically consistent with observations in order to be objectively considered as realistic. To evaluate the reliability metric, we present rank histograms (*Fig.* 3) computed for each grid point by accumulation over all 24 members of the ensemble at four different Longhurst provinces (Longhurst et al., 1995, *Fig.* 1 provides the location of the

provinces). The provinces used are NADR (North Atlantic Drift), NATR (North Atlantic tropical gyre), NASTE (Northeast Atlantic subtropical gyre), and NASTW (Northwest Atlantic subtropical gyre). Both the assimilation analysis and free run ensembles are displayed. Ranks are computed against SeaWiFS ocean color data extracted for the same day with a considered 30% of observation error. In practice, the latter error means that for each realization a Gaussian white noise with a standard deviation of 30% of the satellite Chl-*a* concentration is added to each ensemble member.

Histograms are good indicators of how the assimilation of surface Chl-*a* affects the probability distribution of the ensemble. The histogram for province NADR (*Fig.* 3 first row), which corresponds to a major part of the eastern North Atlantic temperate waters ($\sim$40-60°N; $\sim$10-45°W), displays the good performance of the non-assimilated simulation reproducing the given observations. The histogram is flat except for a slightly tall rank '1' that indicates the highest observations are not included in the spread of the ensemble. When observations are assimilated, the distribution of ranks flattens with respect to the shape of the histogram of the non-assimilated experiment. The shape of the histogram illustrates the ensemble is now able to include the highest values of Chl-*a*, though few ranks accumulate in the left side of the histogram.

An accumulation of ranks forms a dome in the middle of the histogram for province NATR (second row), which corresponds to the southern boundary of the North Atlantic subtropical gyre ($\sim$13-26°N; $\sim$16-75°W). The free run surface map (see *Fig.* 2 middle panels) showed too low values in the northern part of the province, and too high values in the southern part, that differ from the smooth gradient showed by the observations. When ocean colour data is assimilated, ranks' distribution becomes more homogeneous. A moderate dome of ranks in the right side of the histogram still appears, yet the envelope of the ensemble reconciles well with the given observations.

The histogram of the free run shows an accumulation of ranks at the left side, i.e., too many ranks '0', for province NASTE (third row). This is the eastern branch of the subtropical gyre of the North Atlantic that goes roughly from the center of the Atlantic to the east European and African coasts (from 30 to $\sim$44°N). The surface map (*Fig.* 2 middle panels) showed an overestimation of Chl-*a* for most of the region, except for the oligotrophic center of the subtropical gyre where values were almost negligible. When observations are assimilated, the values of the oligotrophic area increased while values closer to the coasts tended to decrease. These corrections are also reflected into the histograms by a re-distribution of the lowest ranks to the right. Nonetheless, improvements are limited, and there is an overpopulated left side of the histogram.

Lastly, the right branch of the North Atlantic subtropical gyre is included within province NASTW ($\sim$30-40°N; $\sim$30-75°W; last row). In this area, the free run histogram shows a strong accumulation of ranks at the left extreme, i.e, the ensemble systematically overestimates observations (positive bias). This under-dispersed shape indicates that the ensemble is unable to cover the lowest observations. In this case, the assimilation of satellite data is unable to improve the reliability of the system. Moreover, the accumulation of lower values not included within the probability distribution of the ensemble increases after assimilation.

To see the time evolution of the reliability of the ensemble in province NADR, *Fig.* 4 shows rank histograms computed at three different periods. A week after the initialization of the experiments, i.e., 19 April 2005, there is an accumulation of ranks in the right side of the free run histogram (negative bias). The assimilation of satellite information redistributes ranks to the left. Yet there is still an underestimation, the probability distribution of the analysis ensemble fits better with observations thus
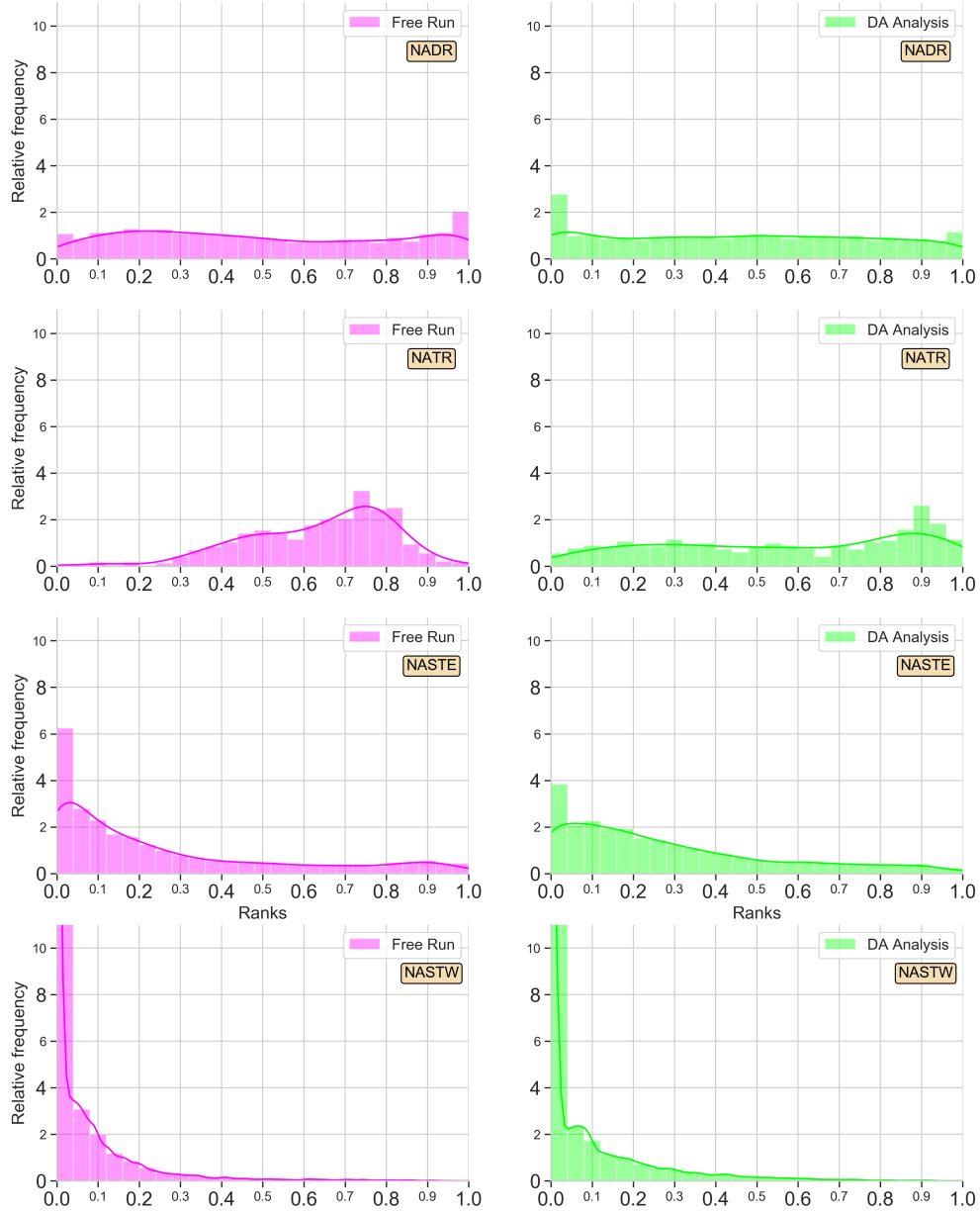
11

Figure 3. Surface Chl-*a* rank histograms of the 24 member free run experiment (magenta; left panels) and the 24 member analysis ensemble assimilation experiment (light green: right panels), in comparison with SeaWiFS data for 15th May 2005. A 30% SeaWiFS observation error is taken into account. Longhurst provinces NADR, NATR, NASTE, and NASTW are represented.

decreasing the bias. A month after, as we observed in *Fig.* 3, both the free run and DA simulations display flat histograms
305   indicating a good performance of the system. In particular, the system reproduces the increasing on Chl-*a* that occurs during
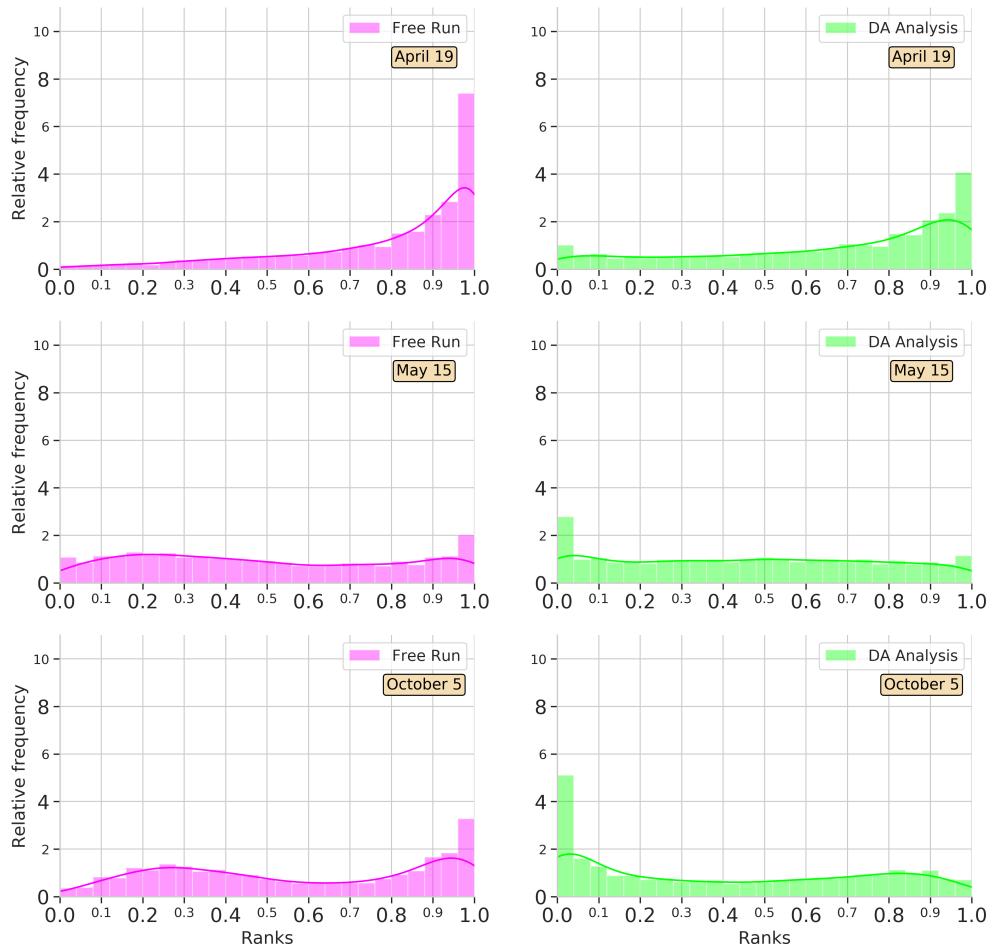
12

Figure 4. Surface Chl-*a* rank histograms of the 24 member free run experiment (magenta; left panels) and the 24 member analysis ensemble assimilation experiment (light green: right panels) in comparison with SeaWiFS data for province NADR. Ranks are computed for 19 April, 15 May, and 5 October 2005. A 30% SeaWiFS observation error is taken into account.

the spring bloom period, which takes place around this date in the province (e.g., Follows and Dutkiewicz, 2001). In October, the free run tends to accumulate ranks on the right side, while an accumulation on the left side of the histogram is depicted for DA analysis. Notwithstanding, the distribution of ranks is more homogeneous after the assimilation process.

To complement reliability measurements, we present an analysis of the CRPS metrics for an in-depth evaluation of the 310 assimilation effects. Using all daily satellite observations available during the simulation period, we calculated the Reli and Reso terms of the CRPS decomposition for provinces NADR and NASTW; two provinces with contrasted behaviours. Rank histograms (*Fig.* 3) showed the ensemble is consistent with observations in NADR while it underestimates them in NASTW. Similarly, the reliability term of the CRPS metric (*Fig.* 5a) shows the improvements (closer to zero) made by the assimilation

13

process on province NADR, in which the prior probability distribution was already coherent with observations. This pattern, however, reverses around August when the integration of data deteriorates the metric. This situation lasts until mid-December, when reliability for both simulations begin to coincide each other until the end of the experiment. By contrast, reliability of the free run simulation is generally closer to zero for province NASTW during the whole experiment.
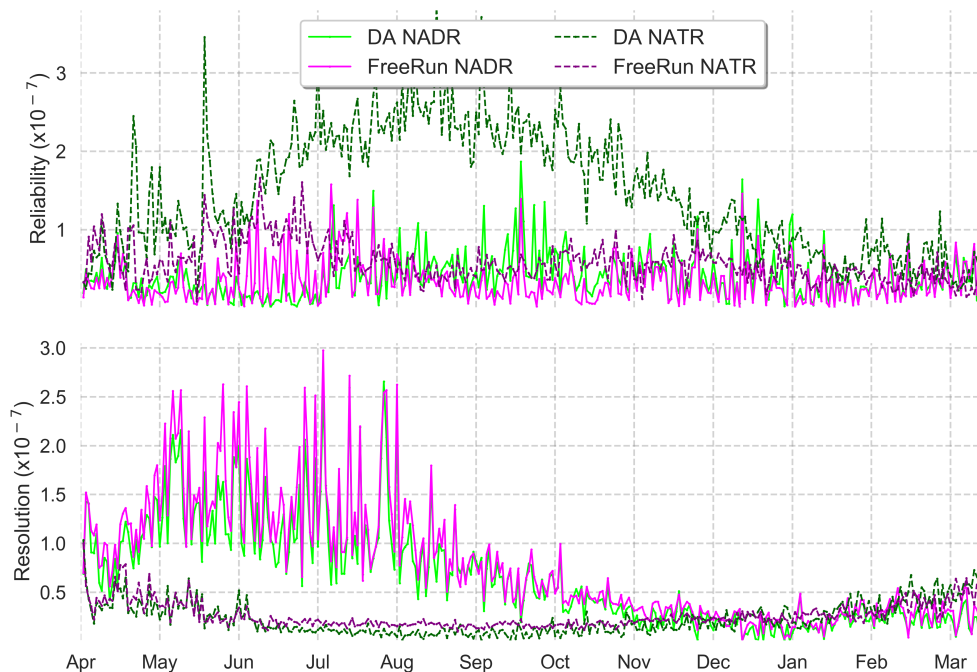

Figure 5. Time series (6th April 2005 to 5th April 2006) of reliability (upper panel) and resolution (lower panel) computed from CRPS decomposition for the 24 member free run (in magenta) and the 24 member forecast ensemble assimilation (in light green) experiments. Longhurst provinces NADR and NASTW are represented.

Time series of the resolution part of CRPS (*Fig.* 5b) show the metric is close to zero for both systems, indicating a good global performance. As expected after precedent metrics diagnostics, the analysis update generally improves the resolution for province NADR. A marked seasonality is observed in the CRPS time series. During summer, the resolution of both simulations increases until the end of the season when it returns back to lower values.

3.3 Assessment of the multivariate scheme

The multivariate scheme employed here allows corrections on surface Chl-*a* to extend to other variables. Considering a complex model such as PISCES, these changes may provoke several variables to no longer satisfy model equations, and thus results produced by these adjustments should be assessed. Moreover, surface corrections both in the observed and non-observed quantities are projected vertically in the water column thus altering the vertical structure of the water column. In order to

14

evaluate the balances between Chl-*a* and those variables that have important relations with it such as nutrients, monthly means of nitrate and phosphate extracted from the WOA2018 data set are compared with data depicted by our simulations. Specifically, vertical profiles of Chl-*a* and nutrient concentrations at two points placed at regions 4 and 6 are presented (*Fig.* 6).
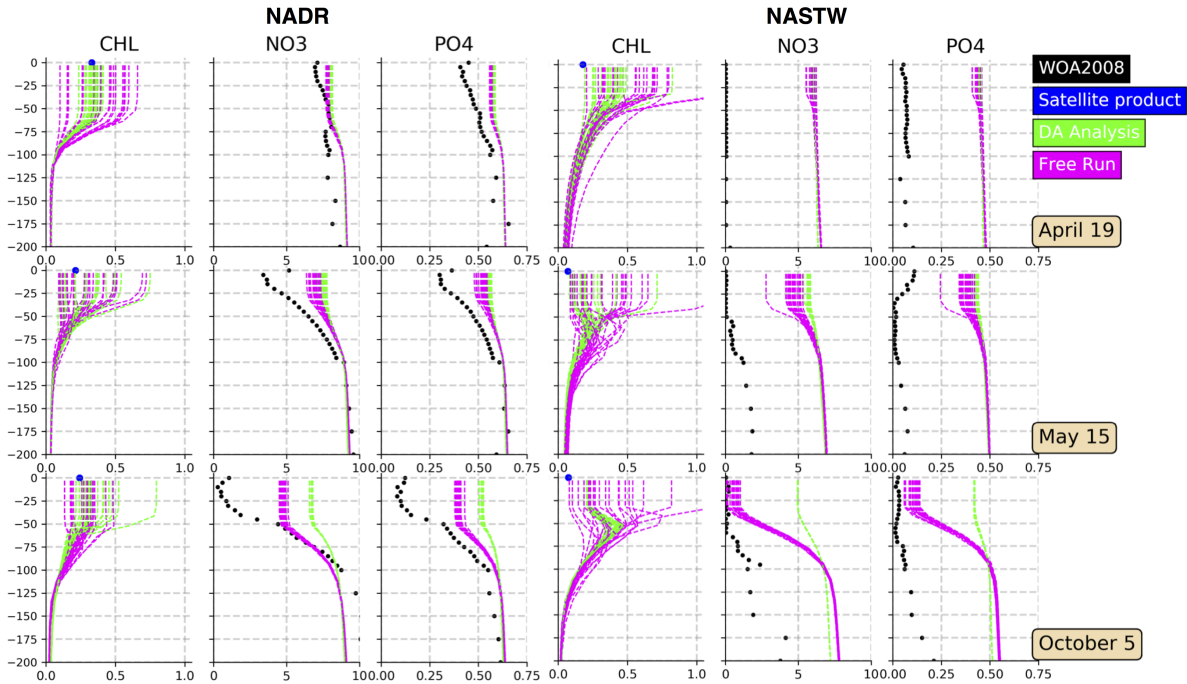

Figure 6. Vertical profiles (0-200 m) of Chl-*a* (mg Chl m^{-3}), nitrate (mmol N m^{-3}) and phosphate (mmol P m^{-3}) for provinces NADR (left panels; at 50° N, 15° W) and NASTW (right panels; at 35° N, 60° W) for 19th April 2005, 15th May 2005, and 5th October 2005. The 24 member free run (in magenta) and analysis (in green) ensembles are represented. Black dots correspond to monthly mean nitrate and phosphate concentrations extracted from WOA2018 database. Blue dots correspond to daily mean surface Chl-*a* obtained from the Global Ocean Satellite Observations.

330   Vertical profiles show that both ensembles are capable of displaying a wide range of Chl-*a* values within the first meters of the water column. As expected, the spread of the analysis reduces while the subsequent forecast (not shown) will restore it accordingly to match the satellite's uncertainty for the next update. The envelopes of both simulations decrease towards the bottom of the mixed layer. From there, concentrations displayed by both simulations coincide. This indicates the extension up to which surface corrections are projected into the vertical. The spread of the ensemble reduces when nutrients are represented.

335   In general, the assimilation process increases their concentrations within the mixed layer.

In province NADR (left panels on *Fig.* 6), the concentrations of nutrients in the mixed layer decrease over time. In October, mixing is close to its lowest (Zhang et al., 2018) and so are nutrients' concentrations. Inferred nutrients follow the seasonal pattern of decreasing towards October. However, their values are relatively high in comparison with climatological data. The

assimilation process tends to further increase nutrient's availability within the mixed layer, yet being capable of correctly simulating surface Chl-*a*.

The water column is poor in nutrients at province NASTW (right panels in *Fig.* 6). However, both simulations show their concentrations to be up to seven times higher than WOA data. Weaknesses on the physical model to appropriately represent the mixed layer dynamics in the region impairs the representation of biogeochemistry as shown in Ourmières et al. (2009). As observed for province NADR, nutrients concentrations decrease towards the end of the summer. The free run simulates this decreasing, especially during October when concentrations are close to observations. By contrast, the analysis moves away the distribution of nutrients from climatology. Corrections made by surface information are unable here to include the given Chl-*a* observations. Surface data is overestimated by both ensembles. The assimilation process approaches the ensemble to observations in the first cycles of assimilation, but it strongly overestimates them in October. The free run shows a too wide spread that reproduces Chl-*a* concentrations up to an order of magnitude higher than satellite data.

3.4   Impact on the subtropical region

Figures presented in precedent sections indicate an erratic behaviour of the system representing the transition zone between the oligotrophic subtropical area and temperate waters northwards. In order to illustrate the vertical distribution of biogeochemical properties before and after assimilation in this area, we consider meridional vertical sections of Chl-*a* crossing the subtropical gyre and temperate waters at 45° W with nutrients (nitrate + ammonium) isolines superimposed (*Fig.* 7). The same three dates used before are represented.

During April (*Fig.* 7a), high values of Chl-*a* deepen up to ∼50 m depth in both experiments. However, the oligotrophic region reaches further north after the assimilation due to a deeper nutrient-depleted subsurface layer south of ∼30° N. The deep Chl-*a* maximum (DCM) of the subtropical region is placed below 100 m depth in both simulations in agreement with observational studies (Pérez et al., 2006). After assimilation, the DCM is disconnected from the subsurface maximum of temperate waters by the vertical slumping of nutrients isolines.

A horizontal strong gradient of nutrient isolines is observed in the DA analysis section of May (*Fig.* 7b). Several patches of high Chl-*a* values are evident south of ∼35° N, from where the water column setting becomes similar to that displayed by the free run simulation. These patches may be caused by the vertical propagation of surface corrections. By contrast, the free run simulation shows a more logical distribution of parameters in which high Chl-*a* waters are related to nutrients' availability.

During October (*Fig.* 7c), differences after assimilation are more noticeable. In this period, the vertical distribution of nutrients has a key role controlling phytoplankton growth in the region (e.g., Dutkiewicz et al., 2001), and concentrations of Chl-*a* are relatively low as the nutricline is deep enough to limit production. Since the free run overestimates Chl-*a* during this period in the region, the assimilation process reduces its concentrations. As a consequence, nutrients accumulate in the first 100 m of the water column north of ∼30° N after the update, and destabilize the equilibrium between the biomass of producers (that decreases) and the availability of nutrients (that increases). Since biogeochemical dynamics is highly dependent on this equilibrium, subsequent forecasts lead to a rapid increase of Chl-*a*, and into a severe overestimation over time that reduces the extension of the oligrotrophic region to the north.
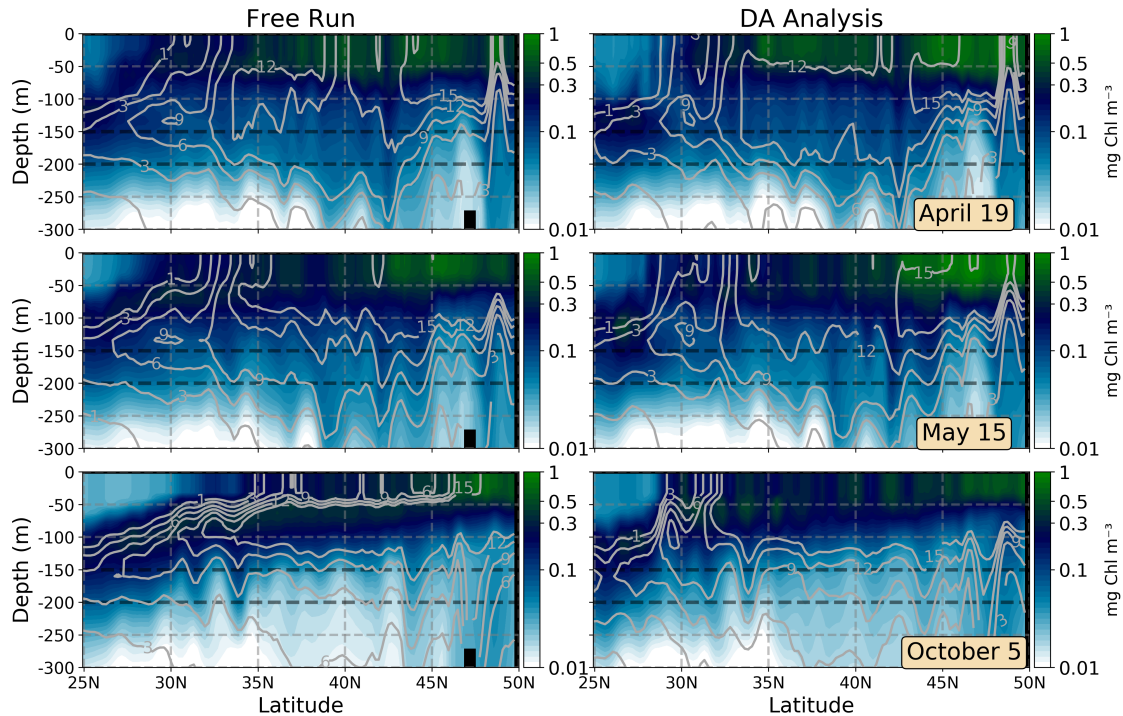
16

Figure 7. Meridional vertical sections (0-300 m) of Chl-*a* (mg Chl m^{-3}) at 45° W, 25 to 50° N, for 19th April 2005, 15th May 2005, and 5th October 2005. The ensemble median of the free run (left panels) and the assimilated (DA Analysis; right panels) simulations are represented. Nitrate+ammonium isolines (mmol N m^{-3}) are included in solid black lines.

4 Discussion

4.1 Impact of the assimilation in the observed variable

375   The North Atlantic ocean is a complex basin that includes a large number of biogeochemical regimes (see *Fig.* 1) that make it difficult to simulate using an holistic modelling system (DeYoung et al., 2004). By employing DA, we aim to reduce the impacts of model errors on the representation of ocean biogeochemistry by combining model information with available observations (Gregg et al., 2009; Ciavatta et al., 2011; Ford and Barciela, 2017). Accordingly, surface maps presented in *Fig.* 2 show that the assimilation process reduces the discrepancies between satellite observations and the non-assimilated free run experiment

380   over a major part of the domain. In particular, the DA simulation better represents values and geographical location of some structures and events such as the spring bloom period, the Gulf Stream, or phytoplankton fronts. By contrast, the assimilation scheme appears to be unable to deal with an unrealistic too abrupt front that separates the oligotrophic and temperate waters conditions (from about 25 to 35°N).

By using rank histograms, we evaluate the capability of the assimilated and the free run ensembles to agree with observations on selected Longhurst provinces (see *Fig.* 3). Histograms illustrate that the response of the system to the assimilation of satellite data depends upon the reliability of the prior ensemble. The assimilation process improves the statistical consistency of the system where the free run probability distribution is homogeneous as in province NADR. The DA process also enhances reliability in those regions where the shape of the free run histogram is over-dispersed as in province NATR. In these regions, the stochastic parameterization is enough to describe properly the variability of the system, and only a relatively small percentage of the observations lie outside of the limits of the ensemble ($\sim$10%). Then, the assimilation process makes use of this information to increase the model skills both by reducing the dispersion and by redistributing ranks to a more homogeneous shape. The redistribution of the ensemble also raises its resolution showing that the posterior ensemble better describes a wide variety of biogeochemical situations (see lower panel of *Fig.* 5).

By contrast, in regions where the prior probability distribution is strongly under-dispersed as in provinces NASTW and NASTE, the assimilation of satellite information is unable to raise the reliability. Since corrections are computed in the range explored by the prior ensemble, the assimilation scheme cannot correct prior distributions that exclude the full variability of the observations. In these provinces, the spread of the prior ensemble is insufficient to represent the range displayed by the observations; the ensemble consistently overestimates them during the annual cycle, and so ranks accumulate at the left extreme of the histograms (positive bias). These two provinces occupy a major part of the oligotrophic subtropical gyre of the North Atlantic where Chl-*a* is generally low during the whole year. Since Chl-*a* values can never become negative, the random perturbations introduced into the model formulation to create a probabilistic simulation (Garnier et al., 2016) preferentially induce to increase Chl-*a* concentrations.

The inability of the assimilation process to improve the skills of the simulation in these latter regions points out the necessity to appropriate define the stochastic parameterizations of the prior PDF as a prerequisite to use DA. Particularly, uncertainties should be described accordingly with the biogeochemical characteristics of each region in order to include a major part of the observation variability.

4.2 Non-observed variables

The effects of the assimilation process to unobserved variables is a major issue in biogeochemical DA (e.g., Rousseaux and Gregg, 2012; Ciavatta et al., 2018). Several studies (e.g., Ciavatta et al., 2011) have found that the integration of surface ocean color may cause problems in the nutrients vertical distribution when model's equation are not 'plastic', in the sense of constraining the ability of the assimilation process to correct the inferred variables. In this regard, it is important to notice that our multivariate analysis scheme allows corrections on five nutrients, the Chl-*a* content of each phytoplankton group, phytoplankton and zooplankton biomasses, and oxygen, while it only uses Chl-*a* satellite data to constrain the ocean biogeochemistry. It is plausible that modifications on biogeochemical variables would make some of them not to comply with the governing model equations anymore. Particularly in those regions where the model is not plastic enough to absorb modifications on the tight correlations between observed and unobserved state vectors. In some cases, these modifications may develop into simulation instabilities that can lead subsequent forecasts to deteriorate both the observed and unobserved variables (Ciavatta et al., 2011,

2018; Gregg et al., 2009). For instance, large discrepancies between observations (high concentrations of Chl-*a*) and the model (lower concentrations) in Gregg (2008) caused their model to become unstable due to nutrient depletion. In the present case, the assimilation process has two effects on the vertical distribution of nutrients (see *Fig.* 6 and *Fig.* 7): (1) it significantly reduces the spread of the ensemble, and (2) it tends to increase their concentrations within the first ∼100 m depth.

Nutrients were not perturbed by the stochastic parameterizations (see Garnier et al., 2016) and so increases during the analysis update cannot be attributed but to the assimilation process. In the northern region of the North Atlantic subtropical gyre, Chl-*a* is overestimated by the prior ensemble and so surface corrections preferentially reduce their concentrations. Since nutrients are negatively correlated with the observed variable, the corrections made by the assimilation process would increase nutrient's availability. Ourmières et al. (2009) observed that the distribution of nitrate controls the biogeochemical dynamics of the subtropical region. As a consequence, the amount of nutrients available in the water column after the analysis would alter the correlations with the observed variable during the subsequent forecast in this area. If the ensemble spread were correctly established in the region, PISCES equations would be capable to absorb these corrections. However, the ensemble has insufficient spread in provinces NASTW and NASTE, and the increasing of nutrients lead to a consistent overestimation of Chl-*a*. By contrast, in the rest of the domain, the parameterizations of the uncertainties are consistent with observations, and extrapolation of the assimilated information to non-observed variables works correctly. The assimilation process increases the reliability of the ensemble, and the information spreads appropriately to the rest of the variables. As a result, the subsequent daily forecast is based on an ensemble that has more appropriate spread thus improving its general performance.

4.3   Assimilation on fluctuations

The previous section has shown that, despite the stochastic parameterization, PISCES equations are still not plastic enough in the region north of the subtropical gyre to produce an ensemble spread that is compatible with the observations, and thus to absorb the corrections made by data assimilation. A possible way to alleviate these inconsistencies without enhancing the stochastic model would be to reduce the ambition of the data assimilation system, and only apply corrections to components of the observation misfit that are compatible with the ensemble spread. This approach requires a procedure to separate all model fields into two components: one component that displays uncertainties that are not correctly represented by the stochastic model, which will be kept untouched by the assimilation scheme, and another component for which the ensemble simulations can be assumed reliable enough to apply ensemble corrections.

In our system, in the region covered by province NASTW, the main reason for which the ensemble spread is not able to include ocean colour observations is a bias in the model climatology, which is left mostly unexplained by the two sources of uncertainties that have been simulated in the stochastic model. A possible approach to reduce the ambition of data assimilation is thus to separate the model field into a climatological component and a fluctuating component, and apply the assimilation process to the fluctuating component only. The main problem is then to define an operator to separate these two components.

The model climatology on the one hand and the observation climatology on the other hand can be both defined as the distribution of all values that a given variable can take over time at a given location, and can be constructed by compiling all values given by the model or by the observations, at that specific location. In practice, these two distributions can be described
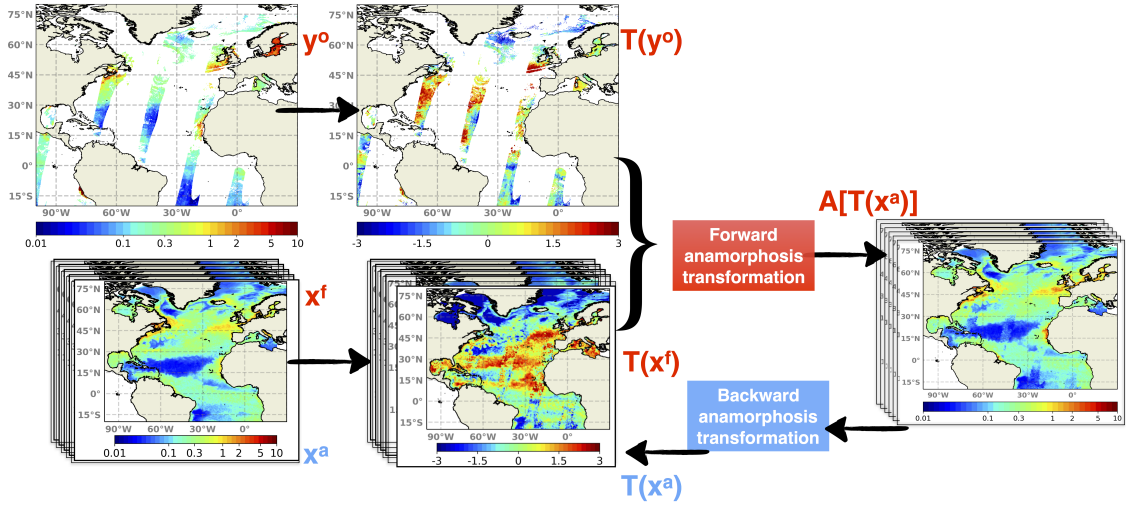
19

Figure 8. Schematics of the assimilation process including time-independent transformations. Both daily ensemble forecast (X^f) and daily satellite observations (y^o) are transformed by their own climatologies. Then, they are projected into the anamorphic space prior of entering the analysis step. After the update, the ensemble analysis (X^a) is converted back to initialize the subsequent daily forecast.

by computing a series of quantiles (for instance deciles), which can be saved as 2D or 3D fields for all model variables on the one hand and for all observed variables on the other hand. The idea is then to keep the model climatology unchanged, and only correct the rank of the model solution within its own climatology, by assimilating the rank of the observation within
455   the observed climatology. This means for instance that if an observation of Chl-*a* falls on the first quartile of the observed climatology, then the model would be corrected to move towards the first quartile of its own climatology. In this way, the fluctuations should be improved, but not the bias between the climatologies, with the expected advantage of not bringing unobserved variables to unrealistic situations.

In practice, a direct solution to extract the fluctuating component is to apply the anamorphic operator transforming the
460   climatological distribution into normalized Gaussian distribution (with zero mean and unit variance). This can be done using the same technique used in the assimilation scheme to transform the prior ensemble into Gaussian marginal distributions. As explained in Brankart et al. (2012), the transformation operator is described by the quantiles of the probability distribution to be transformed (here the climatological distributions). Thus, as explained by the schematics in *Fig.* 8, observations are transformed using the quantiles of the observed climatology, and the prior ensemble is transformed using the quantiles of the
465   model climatology. These two quantities represent the fluctuating component of the system, and the same data assimilation system (described in section 2) can then be applied to this fluctuating component instead of the full field.

A one-month assimilation experiment (TrDA) using this methodology is performed. In order to illustrate the effect of transformations on the ensemble simulation, vertical profiles of Chl-*a*, nitrate, and phosphate are presented for 5th May 2005 (*Fig.* 9), the last day of the experiment. Profiles are placed at province NATSW since the methodology aims to reduce the incon-

470 sistencies between observed and non-observed variables found in this region. Profiles illustrate that the transformed ensemble
keeps the Chl-*a* values displayed by the non-transformed simulation, while it increases the envelope of the ensemble by repro-
ducing lower values. On the other hand, when climatologies are taken into account, the increase of the concentrations of both
nitrate and phosphate after corrections is reduced. However, despite these improvements, we see that, even with the modified
observational update, it is still difficult to maintain the corrections of the nutrients within reasonable bounds. Climatological
475 variations can indeed be too wide to avoid unrealistic values occurring at a given time. Looking for a reliable synoptic ensem-
ble with a sufficient dynamical spread to explain the full misfit to the observations of the day should thus certainly remain an
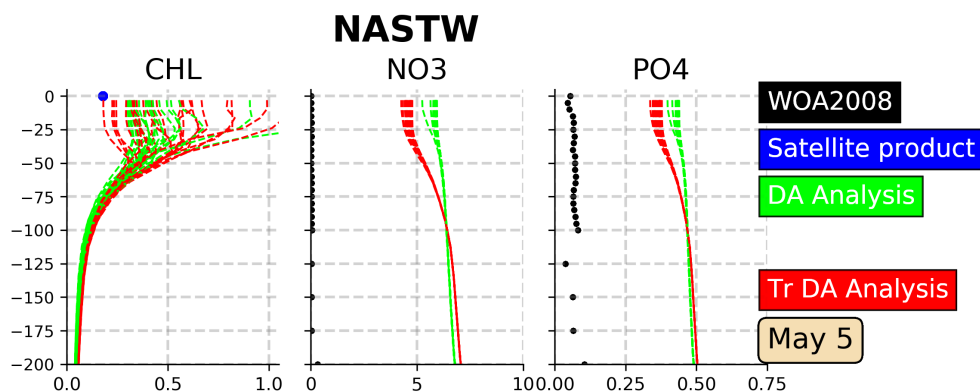important step to improve the assimilation system.

Figure 9. Vertical profiles (0-200 m) of Chl-*a* (mg Chl m^{-3}), nitrate (mmol N m^{-3}) and phosphate (mmol P m^{-3}) at province NASTW (35°
N, 60° W) for 5th May 2005. The 24 member analysis (in green) and the 24 member transformed analysis (in red) ensembles are represented.
Black dots correspond to monthly mean nitrate and phosphate concentrations extracted from WOA2018 database. Blue dots correspond to
daily mean surface Chl-*a* obtained from the Global Ocean Satellite Observations.

5   Summary and conclusions

Satellite-derived surface Chl-*a* data are daily assimilated into a three dimensional 24 member ensemble configuration of a
480 coupled NEMO-PISCES model for the North Atlantic. As shown throughout the text, the assimilated system has brought
us promising results. A regional diagnosis of a one-year assimilation experiment has revealed that the integration of surface
information increases the skills of the ensemble system in a major part of the model grid when compared to an analogous
non-assimilated free run simulation. Particularly, the assimilation of satellite data improves the representation of the surface
Chl-*a* variability both in location (upwelling areas, subtropical gyre, Gulf Stream, etc) and seasonality (spring bloom, winter
485 mixing, etc). Therefore, the stochastic parameterizations introduced into the system by Garnier et al. (2016) have shown to be
adequate for undertaking DA in most of the considered domain. Where the prior ensemble includes the variability shown by
the observations and their uncertainties, the assimilation process improves its probability distribution increasing the agreement

with observations (reliability), and its capability to display different community behaviours (resolution). Moreover, corrections are appropriately transferred to unobserved state vectors by the multivariate scheme.

490   In the northern region of the North Atlantic subtropical gyre, however, the multivariate corrections produce values that are often inconsistent with model dynamics, which can affect the correlations between the biogeochemical variables. In this region, the simulation cannot absorb adequately the corrections brought by the observations, i.e., the simulation is not plastic, and the system's performance deteriorates after the assimilation process. Particularly, the analysis update increases the concentrations of nutrients producing instabilities that lead the subsequent forecast to degrade biogeochemical fields. These results suggest

495   that the description of uncertainties needs to be refined according to the biogeochemical characteristics of each Longhurst province.

One possible approach to reduce these instabilities would be to relax the assimilation effects on those areas. Therefore, we carried out a experiment in which corrections are only applied to the fluctuation part of the model. For that end, we apply transformations both to observations and the forecast ensemble before entering the analysis update using their climatologies.

500   Results from a one-month experiment show that these transformations reduce the strong effects of the assimilation increasing nutrients concentrations in the region that lead to inconsistencies.

In addition, an improved simulation of the dynamics is needed. Ourmières et al. (2009) carried out a detailed analysis on the mixed layer dynamics at mid-latitudes. They observed that the distribution of nitrate controls the biogeochemical dynamics of the subtropical region by employing physical - only , biogeochemical - only (nitrate data), and physical - biogeochemical

505   combined assimilation techniques over a coupled system. Their results showed a too deep mixed layer during March that extended over an abnormally large area in the Gulf Stream region and its north eastern extension, and an overestimation of the stratification in the north-east Atlantic. This biased representation of the dynamics has a significant impact on the present model, and should be addressed in future realizations.

Including information of biogeochemical fields in the water column into the assimilation scheme would also improve the

510   representation of the biogeochemical state of the ocean. *In situ* information would be thus explicitly included by the system at depth. Nowadays, the only sources of such measurements are limited to the prospects of BIO-Argo floats (Claustre, 2009; Xing et al., 2012). Terzić et al. (2018) assimilated BIO-Argo information into a one-dimensional model and improved the DCM spatial and seasonal representation. Cossarini et al. (2019) succeed in improving the Chl-*a* depiction over the Mediterranean Sea by assimilating vertical Chl-*a* information supplied by BIO-Argo floats. These recent works open a horizon to constrain

515   biogeochemical model simulations from vertical information. However, at basin scales, the current state of the network allows it to be used for validation purposes, but their limited spatial coverage makes them insufficient for assimilation procedures. In the other hand, a possibility to include nutrients information is to introduce synthetic information (e.g., Xiao and Friedrichs, 2014; Yu et al., 2018) from a non-perturbed analogue simulation. In this direction, synthetic observations would be important in future efforts heading the improvement of biogeochemical data assimilation systems.

References

525   Anderson, J.: A method for producing and evaluating probabilistic forecasts from ensemble model integrations, Journal of Climate, 9, 1518–
1530, https://doi.org/10.1175/1520-0442(1996)009<1518:AMFPAE>2.0.CO;2, 1996.

Auger, P., Machu, E., Gorgues, T., Grima, N., and Waeles, M.: Comparative study of potential transfer of natural and anthropogenic cadmium to plankton communities in the North-West African upwelling, Science of the Total Environment, 505, 870–888, https://doi.org/10.1016/j.scitotenv.2014.10.045, 2015.

530   Aumont, O., Éthé, C., Tagliabue, A., Bopp, L., and Gehlen, M.: PISCES-v2: an ocean biogeochemical model for carbon and ecosystem studies, Geoscientific Model Development Discussions, 8, https://doi.org/10.5194/gmdd-8-1375-2015, 2015.

Barnier, B., Madec, G., Penduff, T., Molines, J., Treguier, A., Le Sommer, J., Beckmann, A., Biastoch, A., Böning, C., Dengg, J., Derval, C., Durand, E., Gulev, S., Remy, E., Talandier, C., Theetten, S., Maltrud, M., McClean, J., and De Cuevas, B.: Impact of partial steps and momentum advection schemes in a global ocean circulation model at eddy-permitting resolution, Ocean dynamics, 56, 543–567,
535   https://doi.org/10.1007/s10236-006-0082-1, 2006.

Béal, D., Brasseur, P., Brankart, J., Ourmières, Y., and Verron, J.: Characterization of mixing errors in a coupled physical biogeochemical model of the North Atlantic: implications for nonlinear estimation using Gaussian anamorphosis, Ocean Science, 6, 247–262, https://doi.org/10.5194/os-6-247-2010, 2010.

Berner, J., Achatz, U., Batté, L., Bengtsson, L., Cámara, A., Christensen, H., Colangeli, M., Coleman, D., Crommelin, D., Dolaptchiev, S.,
540   Franzke, C., Friederichs, P., Imkeller, P., Järvinen, H., Juricke, S., Kitsios, V., Lott, F., Lucarini, V., Mahajan, S., Palmer, T., Penland, C., Sakradzija, M., von Storch, J., Weisheimer, A., Weniger, M., Williams, P., and Yano, J.: Stochastic parameterization: Toward a new view of weather and climate models, Bulletin of the American Meteorological Society, 98, 565–588, https://doi.org/10.1175/BAMS-D-15-00268.1, 2017.

Bertino, L., Evensen, G., and Wackernagel, H.: Sequential data assimilation techniques in oceanography, International Statistical Review, 71,
545   223–241, https://doi.org/10.1111/j.1751-5823.2003.tb00194.x, 2003.

Bessières, L., Leroux, S., Brankart, J., Molines, J., Moine, M., Bouttier, P., Penduff, T., Terray, L., Barnier, B., and Sérazin, G.: Development of a probabilistic ocean modelling system based on NEMO 3.5: Application at eddying resolution, Geoscientific Model Development, 10, 1091–1106, https://doi.org/10.5194/gmd-10-1091-2017, 2017.

Bopp, L., Lévy, M., Resplandy, L., and Sallée, J. B.: Pathways of anthropogenic carbon subduction in the global ocean, Geophysical Research
550   Letters, 42, 6416–6423, https://doi.org/10.1002/2015GL065073, 2015.

Boyer, T., Antonov, J., Baranova, O., Coleman, C., Garcia, H., Grodsky, A., Johnson, D., Locarnini, R., Mishonov, A., O'Brien, T., Paver, C., Reagan, J., Seidov, D., Smolyar, I., and Zweng, M.: World Ocean Database 2013, 2013.

Brankart, J., Testut, C., Béal, D., Doron, M., Fontana, C., Meinvielle, M., Brasseur, P., and Verron, J.: Towards an improved description of ocean uncertainties: effect of local anamorphic transformations on spatial correlations, Ocean Science, 8, 121, https://doi.org/10.5194/os-
555   8-121-2012, 2012.

Brankart, J., Candille, G., Garnier, F., Calone, C., Melet, A., Bouttier, P., Brasseur, P., and Verron, J.: A generic approach to explicit simulation of uncertainty in the NEMO ocean model, Geoscientific Model Development, 8, 1285–1297, https://doi.org/10.5194/gmd-8-1285-2015, 2015.

Brasseur, P. and Verron, J.: The SEEK filter method for data assimilation in oceanography: a synthesis, Ocean Dynamics, 56, 650–661,
560   https://doi.org/10.1007/s10236-006-0080-3, 2006.

Brasseur, P., Gruber, N., Barciela, R., Brander, K., Doron, M., Elmoussaoui, A., Hobday, A., Huret, M., Kremeur, A., Lehodey, P., et al.: Integrating biogeochemistry and ecology into ocean data assimilation systems, Oceanography, 22, 206–215, 2009.

Buizza, R., Milleer, M., and Palmer, T.: Stochastic representation of model uncertainties in the ECMWF ensemble prediction system, Quarterly Journal of the Royal Meteorological Society, 125, 2887–2908, https://doi.org/10.1002/qj.49712556006, 1999.

565　Campbell, J.: The lognormal distribution as a model for bio-optical variability in the sea, Journal of Geophysical Research: Oceans, 100, 13 237–13 254, https://doi.org/10.1029/95JC00458, 1995.

Candille, G., Brankart, J., and Brasseur, P.: Assessment of an ensemble system that assimilates Jason-1/Envisat altimeter data in a probabilistic model of the North Atlantic ocean circulation, Ocean Science, 11, 425–438, https://doi.org/10.5194/os-11-425-2015, 2015.

Ciavatta, S., Torres, R., Saux-Picart, S., and Allen, J.: Can ocean color assimilation improve biogeochemical hindcasts in shelf seas?, Journal

570　of Geophysical Research: Oceans, 116, https://doi.org/10.1029/2011JC007219, 2011.

Ciavatta, S., Brewin, R., Skakala, J., Polimene, L., de Mora, L., Artioli, Y., and Allen, J.: Assimilation of ocean-color plankton functional types to improve marine ecosystem simulations, Journal of Geophysical Research: Oceans, 123, 834–854, https://doi.org/10.1002/2017JC013490, 2018.

Claustre, H.: Bio-optical profiling floats as new observational tools for biogeochemical and ecosystem studies: Potential synergies with ocean

575　color remote sensing, https://doi.org/10.5270/OceanObs09.cwp.17, 2009.

Cossarini, G., Mariotti, L., Feudale, L., Mignot, A., Salon, S., Taillandier, V., Teruzzi, A., and D'Ortenzio, F.: Towards operational 3D-Var assimilation of chlorophyll Biogeochemical-Argo float data into a biogeochemical model of the Mediterranean Sea, Ocean Modelling, 133, 112–128, https://doi.org/10.1016/j.ocemod.2018.11.005, 2019.

Dee, D., Uppala, S., Simmons, A., Berrisford, P., Poli, P., Kobayashi, S., Andrae, U., Balmaseda, M., Balsamo, G., Bauer, P., et al.: The

580　ERA-Interim reanalysis: configuration and performance of the data assimilation system, https://doi.org/10.1002/qj.828, 2011.

DeYoung, B., Heath, M., Werner, F., Chai, F., Megrey, B., and Monfray, P.: Challenges of modeling ocean basin ecosystems, Science, 304, 1463–1466, https://doi.org/10.1126/science.1094858, 2004.

Doron, M., Brasseur, P., and Brankart, J.: Stochastic estimation of biogeochemical parameters of a 3D ocean coupled physical–biogeochemical model: Twin experiments, Journal of Marine Systems, 87, 194–207, https://doi.org/10.1016/j.jmarsys.2011.04.001, 2011.

585　Doron, M., Brasseur, P., Brankart, J., Losa, S., and Melet, A.: Stochastic estimation of biogeochemical parameters from Globcolour ocean colour satellite data in a North Atlantic 3D ocean coupled physical–biogeochemical model, Journal of Marine Systems, 117, 81–95, https://doi.org/10.1016/j.jmarsys.2013.02.007, 2013.

Dutkiewicz, S., Follows, M., Marshall, J., and Gregg, W.: Interannual variability of phytoplankton abundances in the North Atlantic, Deep Sea Research Part II: Topical Studies in Oceanography, 48, 2323–2344, https://doi.org/10.1016/S0967-0645(00)00178-8, 2001.

590　Elmoussaoui, A., Perruche, C., Greiner, E., Ethé, C., and Gehlen, M.: Integration of biogeochemistry into Mercator Ocean systems, Mercator Ocean newsletter, 40, 3–14, 2011.

Fennel, K., Gehlen, M., Brasseur, P., Brown, C., Ciavatta, S., Cossarini, G., Crise, A., Edwards, C., Ford, D., Friedrichs, M., Gregoire, M., Jones, E., Kim, H., Lamouroux, J., Murtugudde, R., and Perruche, C.: Advancing Marine Biogeochemical and Ecosystem Reanalyses and Forecasts as tools for monitoring and managing Ecosystem Health, Frontiers in Marine Science, 6, 1–9,

595　https://doi.org/10.3389/fmars.2019.00089, 2019.

Follows, M. and Dutkiewicz, S.: Meteorological modulation of the North Atlantic spring bloom, Deep Sea Research Part II: Topical Studies in Oceanography, 49, 321–344, https://doi.org/10.1016/S0967-0645(01)00105-9, 2001.

25

Fontana, C., Brasseur, P., and Brankart, J.: Toward a multivariate reanalysis of the North Atlantic Ocean biogeochemistry during 1998–2006 based on the assimilation of SeaWiFS chlorophyll data, Ocean Science, 9, 37–56, https://doi.org/10.5194/os-9-37-2013, 2013.

Ford, D. and Barciela, R.: Global marine biogeochemical reanalyses assimilating two different sets of merged ocean colour products, Remote Sensing of Environment, 203, 40–54, https://doi.org/10.1016/j.rse.2017.03.040, 2017.

Ford, D. A., Edwards, K., Lea, D., Barciela, R., Martin, M., and Demaria, J.: Assimilating GlobColour ocean colour data into a pre-operational physical-biogeochemical model, Ocean Science, 8, 751–771, https://doi.org/10.5194/os-8-751-2012, 2012.

Garcia, H. E., Weathers, K. W., Paver, C. R., Smolyar, I., Boyer, T., Locarnini, R., Zweng, M., Mishonov, A., Baranova, O. K., Seidov, D., and Reagan, J.: NOAA Atlas NESDIS 84 WORLD OCEAN ATLAS 2018 Volume 4: Dissolved Inorganic Nutrients (phosphate, nitrate and nitrate+nitrite, silicate), World Ocean Atlas 2018, 4, 2019.

Garnier, F., Brankart, J., Brasseur, P., and Cosme, E.: Stochastic parameterizations of biogeochemical uncertainties in a $1/4°$ NEMO/PISCES model for probabilistic comparisons with ocean color data, Journal of Marine Systems, 155, 59–72, https://doi.org/10.1016/j.jmarsys.2015.10.012, 2016.

Geider, R., MacIntyre, H., and Kana, T.: Dynamic model of phytoplankton growth and acclimation: responses of the balanced growth rate and the chlorophyll a: carbon ratio to light, nutrient-limitation and temperature, Marine Ecology Progress Series, 148, 187–200, https://doi.org/10.3354/meps148187, 1997.

Germineaud, C., Brankart, J., and Brasseur, P.: An ensemble-based probabilistic score approach to compare observation scenarios: an application to biogeochemical-Argo deployments, Journal of Atmospheric and Oceanic Technology, https://doi.org/10.1175/JTECH-D-19-0002.1, 2019.

Gregg, W.: Assimilation of SeaWiFS ocean chlorophyll data into a three-dimensional global ocean model, Journal of Marine Systems, 69, 205–225, https://doi.org/10.1016/j.jmarsys.2006.02.015, 2008.

Gregg, W. and Casey, N.: Global and regional evaluation of the SeaWiFS chlorophyll data set, Remote Sensing of Environment, 93, 463–479, https://doi.org/10.1016/j.rse.2003.12.012, 2004.

Gregg, W., Friedrichs, M., Robinson, A., Rose, K., Schlitzer, R., Thompson, K., and Doney, S.: Skill assessment in ocean biological data assimilation, Journal of Marine Systems, 76, 16–33, https://doi.org/10.1016/j.jmarsys.2008.05.006, 2009.

Hersbach, H.: Decomposition of the continuous ranked probability score for ensemble prediction systems, Weather and Forecasting, 15, 559–570, https://doi.org/10.1175/1520-0434(2000)015<0559:DOTCRP>2.0.CO;2, 2000.

Houghton, J., Ding, Y., Griggs, D., Noguer, M., van der Linden, P., Dai, X., Maskell, K., and Johnson, C.: Climate change 2001: the scientific basis, The Press Syndicate of the University of Cambridge, 2001.

Jose, Y., Aumont, O., Machu, E., Penven, P., Moloney, C., and Maury, O.: Influence of mesoscale eddies on biological production in the Mozambique Channel: Several contrasted examples from a coupled ocean-biogeochemistry model, Deep Sea Research Part II: Topical Studies in Oceanography, 100, 79–93, https://doi.org/10.1016/j.dsr2.2013.10.018, 2014.

Juricke, S., Palmer, T., and Zanna, L.: Stochastic subgrid-scale ocean mixing: impacts on low-frequency variability, Journal of Climate, 30, 4997–5019, https://doi.org/10.1175/JCLI-D-16-0539.1, 2017.

Lahoz, W., Khattatov, B., and Ménard, R.: Data assimilation: making sense of observations, Part I: Theory, in: Data Assimilation, Springer, 2010.

Le Fouest, V., Zakardjian, B., Saucier, F., and Cizmeli, S.: Application of SeaWIFS- and AVHRR-derived data for mesoscale and regional validation of a 3-D high-resolution physical–biological model of the Gulf of St. Lawrence (Canada), Journal of Marine Systems, 60, 30–50, https://doi.org/10.1016/j.jmarsys.2005.11.008, 2006.

Lefort, S., Aumont, O., Bopp, L., Arsouze, T., Gehlen, M., and Maury, O.: Spatial and body-size dependent response of marine pelagic communities to projected global climate change, Global Change Biology, 21, 154–164, https://doi.org/10.1111/gcb.12679, 2015.

Leutbecher, M., Lock, S., Ollinaho, P., Lang, S., Balsamo, G., Bechtold, P., Bonavita, M., Christensen, H., Diamantakis, M., Dutra, E., English, S., Fisher, M., Forbes, R., Goddard, J., Haiden, T., Hogan, R., Juricke, S., Lawrence, H., MacLeod, D., Magnusson, L., Malardel,

640   S., Massart, S., Sandu, I., Smolarkiewicz, P., Subramanian, A., Vitart, F., Wedi, N., and Weisheimer, A.: Stochastic representations of model uncertainties at ECMWF: State of the art and future vision, Quarterly Journal of the Royal Meteorological Society, 143, 2315–2339, https://doi.org/10.1002/qj.3094, 2017.

Levitus, S., Boyer, T., Conkright, M., O'brien, T., Antonov, J., Stephens, C., Stathoplos, L., Johnson, D., and Gelfeld, R.: NOAA Atlas NESDIS 18, World Ocean Database 1998: vol. 1: Introduction, US Government Printing Office, Washington DC, 346, 1998.

645   Lévy, M., Iovino, D., Resplandy, L., Klein, P., Madec, G., Tréguier, A., Masson, S., and Takahashi, K.: Large-scale impacts of submesoscale dynamics on phytoplankton: Local and remote effects, Ocean Modelling, 43, 77–93, https://doi.org/10.1016/j.ocemod.2011.12.003, 2012.

Longhurst, A., Sathyendranath, S., Platt, T., and Caverhill, C.: An estimate of global primary production in the ocean from satellite radiometer data, Journal of plankton Research, 17, 1245–1271, https://doi.org/10.1093/plankt/17.6.1245, 1995.

Madec, G. et al.: NEMO ocean engine, 2015.

650   Mattern, J. P., Song, H., Edwards, C., Moore, A., and Fiechter, J.: Data assimilation of physical and chlorophyll a observations in the California Current System using two biogeochemical models, Ocean Modelling, 109, 55–71, https://doi.org/10.1016/j.ocemod.2016.12.002, 2017.

Mélin, F., Sclep, G., Jackson, T., and Sathyendranath, S.: Uncertainty estimates of remote sensing reflectance derived from comparison of ocean color satellite data sets, Remote sensing of environment, 177, 107–124, https://doi.org/10.1016/j.rse.2016.02.014, 2016.

655   Oschlies, A. and Garçon, V.: Eddy-induced enhancement of primary production in a model of the North Atlantic Ocean, Nature, 394, 266–269, https://doi.org/10.1038/28373, 1998.

Ourmières, Y., Brasseur, P., Lévy, M., Brankart, J., and Verron, J.: On the key role of nutrient data to constrain a coupled physical–biogeochemical assimilative model of the North Atlantic Ocean, Journal of Marine Systems, 75, 100–115, https://doi.org/10.1016/j.jmarsys.2008.08.003, 2009.

660   Palmer, T.: Towards the probabilistic Earth-system simulator: a vision for the future of climate and weather prediction, Quarterly Journal of the Royal Meteorological Society, 138, 841–861, https://doi.org/10.1002/qj.1923, 2012.

Pérez, V., Fernández, E., Marañón, E., Morán, X., and Zubkov, M.: Vertical distribution of phytoplankton biomass, production and growth in the Atlantic subtropical gyres, Deep-Sea Research Part I: Oceanographic Research Papers, 53, 1616–1634, https://doi.org/10.1016/j.dsr.2006.07.008, 2006.

665   Pham, D., Verron, J., and Roubaud, M.: A singular evolutive extended Kalman filter for data assimilation in oceanography, Journal of Marine systems, 16, 323–340, https://doi.org/10.1016/S0924-7963(97)00109-7, 1998.

Rousseaux, C. and Gregg, W.: Climate variability and phytoplankton composition in the Pacific Ocean, Journal of Geophysical Research: Oceans, 117, https://doi.org/10.1029/2012JC008083, 2012.

Simmons, A.: ERA-Interim: New ECMWF reanalysis products from 1989 onwards, ECMWF newsletter, 110, 25–36, 2006.

670   Teruzzi, A., Bolzon, G., Salon, S., Lazzari, P., Solidoro, C., and Cossarini, G.: Assimilation of coastal and open sea biogeochemical data to improve phytoplankton simulation in the Mediterranean Sea, Ocean Modelling, 132, 46–60, https://doi.org/10.1016/j.ocemod.2018.09.007, 2018.

Terzić, E., Lazzari, P., Organelli, E., Solidoro, C., Salon, S., D'Ortenzio, F., and Conan, P.: Merging bio-optical data from Biogeochemical-Argo floats and models in marine biogeochemistry, Biogeosciences Discussions, pp. 1–32, https://doi.org/10.5194/bg-2018-307, 2018.

675 Toth, Z., Talagrand, O., Candille, G., and Zhu, Y.: Probability and ensemble forecasts, 2003.

von Schuckmann, K., Le Traon, P., Smith, N., Pascual, A., Djavidnia, S., Gattuso, J., Grégoire, M., Nolan, G., Aaboe, S., Aguiar, E., et al.: Copernicus Marine Service Ocean State Report, Issue 3, Journal of Operational Oceanography, 12, S1–S123, https://doi.org/10.1080/1755876X.2019.1633075, 2019.

Xiao, Y. and Friedrichs, M.: The assimilation of satellite-derived data into a one-dimensional lower trophic level marine ecosystem model, Journal of Geophysical Research: Oceans, 119, 2691–2712, https://doi.org/10.1002/2013JC009433, 2014.

680

Xing, X., Zhao, D., Claustre, H., et al.: A new autonomous observation platform of marine biogeochemistry: Bio-Argo floats, Marine Environmental Science, 5, 733–739, 2012.

Yu, L., Fennel, K., Bertino, L., El Gharamti, M., and Thompson, K. R.: Insights on multivariate updates of physical and biogeochemical ocean variables using an Ensemble Kalman Filter and an idealized model of upwelling, Ocean Modelling, 126, 13 – 28, https://doi.org/10.1016/j.ocemod.2018.04.005, 2018.

685

Zhang, Y., Xu, H., Qiao, F., and Dong, C.: Seasonal variation of the global mixed layer depth: comparison between Argo data and FIO-ESM, Frontiers of Earth Science, 12, 24–36, https://doi.org/10.1007/s11707-017-0631-6, 2018.